ARTICLE

Cardiac Rehabilitation by Pulmonary Artery Banding after Induced Dilated Cardiomyopathy: A Pilot Study on a Rodent Model

Domenico Crea[1], Arben Dedja[1], Matteo Ponzoni[1,2], Stefania Rizzo[3], Alberto Cipriani[4], Riccardo Bariani[4], Kalliopi Pilichou[3], Maria Bueno Marinas[3], Danila Azzolina[5] and Massimo A. Padalino[1,6,*]

[1]Pediatric and Congenital Cardiac Surgery, Department of Cardiothoracic and Vascular Sciences and Public Health, University of Padova, Padova, 35128, Italy

[2]Division of Cardiac Surgery, The Sick Children's Hospital, Toronto, ON M5G 1E8, Canada

[3]Cardiovascular Pathology, Department of Cardiothoracic and Vascular Sciences and Public Health, University of Padova, Padova, 35128, Italy

[4]Cardiology Clinic, Department of Cardiothoracic and Vascular Sciences and Public Health, University of Padova, Padova, 35128, Italy

[5]Department of Environmental and Preventive Science, University of Ferrara, Ferrara, 44121, Italy

[6]Department Precision and Regenerative Medicine and Jonian Area, University of Bari "Aldo Moro", Bari, 70124, Italy

*Corresponding Author: Massimo A. Padalino. Email: massimo.padalino@uniba.it

Received: 05 August 2024   Accepted: 25 November 2024   Published: 31 December 2024

ABSTRACT

Background: Since 2015, the pulmonary artery banding (PAB), following the Giessen protocol, has treated end-stage heart failure in selected infants with preserved right ventricular function, acting as a bridge to transplant or recovery, as a result of ventricular-ventricular interaction. **Objectives:** To elucidate whether PAB is a feasible and reproducible procedure in a rodent model of pharmacologically induced dilated cardiomyopathy (DCM) and to evaluate PAB-induced ventricular rehabilitation. **Methods:** We used 49 Sprague-Dawley rats divided into four groups: a sham surgery control group, a healthy animal group undergoing PAB, a doxorubicin (DOX)- treated control group, and a DOX + PAB-treated group. All underwent echocardiographic, histological, and molecular analyses. **Results:** Preliminary results showed high mortality in rats with DOX-induced DCM, with contractile dysfunction confirmed by 2D echocardiography. Signs of damage were detected through transmission electron microscopy, but not via standard histological/molecular tests. PAB after DOX improved contractile function, enhancing ejection fraction ($p = 0.01$) and fractional shortening ($p = 0.03$). **Conclusion:** The DOX-induced DCM model, while reproducible, may not reflect DCM's true pathology. High mortality and individual variability limited the study. Further research is needed to find alternative models with lower mortality and to explore the PAB-induced molecular signaling pathways and cardiac proliferation potential.

KEYWORDS

Dilated cardiomyopathy; doxorubicin; pulmonary artery banding

Nomenclature

DCM	Dilated cardiomyopathy
HF	Heart failure
PAB	Pulmonary artery banding
DOX	Doxorubicin

1 Introduction

Pediatric heart failure (HF) results from various conditions, including genetic, infectious, toxic, or idiopathic factors. It manifests through characteristic signs and symptoms such as oedema, respiratory distress, failure to thrive, and exercise intolerance, all associated with circulatory, neurohormonal, and molecular derangements [1].

While most pediatric heart failure cases are linked to congenital heart diseases, cardiomyopathy, particularly dilated cardiomyopathy (DCM) with preserved right ventricle (RV) function, stands as the second most common cause. In contrast to HF secondary to congenital heart diseases, children with DCM face a grim prognosis, with a 5-year risk for death or cardiac transplantation reaching around 50% for DCM patients [2]. Furthermore, the scarcity of donors restricts transplantation to few selected children. Despite the feasibility of mechanical cardiac support in pediatric patients, complications during support remain consistent, significantly threatening clinical. While a substantial body of research exists on adult HF management, comparable studies in children, particularly infants, are lacking. Personalized HF treatment in children is warranted based on current knowledge from bench to bedside. The pathognomonic aspect of DCM cardiac remodeling, involves abnormal ventricular architecture and chamber configuration (increased volume, adopting a spheroidal shape instead of the normal egg shape), driven histologically by pathologic myocyte hypertrophy, myocyte apoptosis, myofibroblast proliferation, and interstitial fibrosis [3].

Derived from the concept of retraining of the subpulmonary ventricle in congenitally corrected transposition of great arteries, Schranz et al. [4] first reported in 2007 the case of a 2-month-old infant with progressive idiopathic DCM treated with pulmonary artery banding (PAB) at the Giessen Institution. This infant, listed for heart transplantation, experienced a dramatic recovery from end-stage heart failure following PAB. Repositioning of the ventricular septum is a consequence of PAB-induced increase in RV contractility (Anrep effect), wall stress and hypertrophy. This results in an immediate RV-left ventricle (LV) crosstalk, leading to the rehabilitation of LV shape (from spherical to ellipsoid morphology), with reduction of left ventricular end diastolic volume, improved function, and a reduction in mitral regurgitation. The global experience of PAB treatment for end-stage LV-DCM with preserved RV function [5], has reported satisfactory clinical outcomes.

Since 2015, our center has implemented the Giessen methodology, demonstrating it to be an effective strategy for avoiding or delaying heart transplantation in select infants with DCM and preserved RV function. We propose that geometric adjustments of left ventricular dimensions, achieved by realigning the interventricular septum (IVS), can gradually restore left ventricular ejection fraction (EF) [5]. Given these clinical successes, pulmonary artery banding (PAB) could represent a significant advancement in managing select children with end-stage heart failure, especially in resource-limited countries, where other options, such as mechanical support and heart transplantation with consequent immunosuppressive drugs, are prohibitively expensive. However, many questions remain regarding the biological pathways activated by PAB, and several surgical institutions are hesitant to adopt this procedure due to a lack of comprehensive information. A deeper understanding of the efficacy of this technique and its underlying cellular and molecular mechanisms is crucial to providing evidence-based support for PAB as an effective alternative treatment for pediatric heart failure.

In previous experimental attempts involving PAB on doxorubicin (DOX)-induced HF, Yerebakan et al. [6] proposed an innovative experimental sheep model of LV failure generated by intermittent intracoronary injections of DOX, treated with PAB. Researchers choose animal models based on specific aspects of cardiac function to be investigated and the relevance of the findings to human physiology. Each model has its advantages and limitations, with the choice depending on specific experiences, research goals, and ethical considerations.

Our study aimed to investigate, for the first time, in a pilot experiment, whether PAB is a feasible and reproducible procedure in a rodent model of pharmacologically induced DCM and to evaluate PAB-induced ventricular rehabilitation.

2 Methods

2.1 Animals

Forty-nine Sprague-Dawley (SD) male rats were included in this experimental study and were provided by "Envigo RMS Srl" (Milan, Italy). The animals were subdivided into four groups as described in Table 1. All animals were kept under standard laboratory conditions (22 ± 2°C at room temperature, 55 ± 5% humidity, 12 h light-dark cycle) and acclimatized for at least one week before surgery [7]. The study was approved by the Local Ethical Committee (Body for Animal Welfare of the University of Padua) and received Ministerial Authorization (no. 24/2021-PR, released on 14 January 2021).

Table 1: Experimental groups

Procedure	n	Age at procedure (weeks; median-IQR)
SHAM	9	13*
DOX-injection	16	11.5; (9.5–12.7)
PAB	9	12*
DOX-injection + PAB	15	12.6; (9–13.3)

Note: *All the rats inside the group have the same age.

2.2 Anaesthesiologic Protocol for Surgery

As previously described by our Institution [8], fifteen minutes prior to surgery, rats were treated with subcutaneous injections of the analgesic Tramadol (CONTRAMAL®, Forementi Srl, Milano, Italy). For the anaesthesia induction, a filtered vaporizer fluovac sevoflurane/halotane (Harvard Apparatus Ltd., Kent, England) was used, pumping 4% sevoflurane (SEVORANE, Abbott SpA, Campoverde, Italy) into a Plexiglas box, together with an oxygen flow of 1 L/min. Once asleep, animals were kindly pulled out of the box and underwent oro-tracheal intubation through a 16 G cannula. After intubation, animals were ventilated with 1 L/min of oxygen and 2.5% Sevoflurane, using the Rodent Ventilator 7025 (Ugo Basile, Italy). The parameters were set as follows: respiratory frequency (RF) = 65–75 breathes per minute; FiO_2 = 100%; PEEP, 2 cmH_2O; and PEAK, 12 cmH_2O. To avoid the risk of pneumothorax, a 14 G needle-cannula connected to a syringe was frequently left in the chest at negative pressure until the last muscle suture was completed. After chest, muscle, and skin closure, halogenated anesthetic administration was ultimately suspended, and the tracheal cannula was removed with resumption of spontaneous ventilation.

2.3 Procedures

2.3.1 DOX Injections

Among the various protocols described in the literature, we chose a short-term protocol for practical reasons. This protocol consists of six intraperitoneal injections of DOX (2.5 mg/0.5 mL/kg i.p.) every

other day for two weeks, totaling a cumulative dose of 15 mg/kg [9,10]. This approach allows for a shorter duration of the experiment and reduces overall costs. The DOX-injection was done under The Esco Airstream® Class II Microbiological Safety Cabinet (AC2-4S model), with the use of proper personal protective equipment to protect eyes, face and skin. During the follow-up, the animals underwent blood sampling (100 µL) through tail vein puncture. Gene and microRNA expression analysis were undertaken as part of the experimental design. No significant differences were observed compared with PAB treated animals of the same age, sex and strain.

2.3.2 Pulmonary Artery Banding

PAB was performed as previously described [11], with the help of a stereomicroscope M400E (Leica Microsystems Italia srl, Milano, Italy), with 6× and 10× magnification, using a micro-surgery set of instruments and sutures. After trichotomy and a standard skin preparation, a left-anterolateral thoracotomy was practiced in the 3rd intercostal space under general anaesthesia. Then, the pericardium was opened by pulling it up to avoid heart's injury, the left lung was pushed to the side using a sponge gauze. Once the main pulmonary artery and the aorta were recognized and isolated (Fig. 1A), curved forceps were passed between them in order to encircle the main pulmonary artery with the band (Fig. 1B), which consisted of a 2-0 silk suture thread. Once the extremities of the thread were located on the anterior wall of the main pulmonary artery, they were placed near and tied together with a 7-0 Prolene suture in order to tight the band, whose length was preoperatively decided (3.5 mm for young and 4.5 mm for adult rats). Then chest, muscles and skin were closed through 3-0 and 4-0 sutures. During the surgery, blood samples (100 µL) were collected through tail vein puncture.
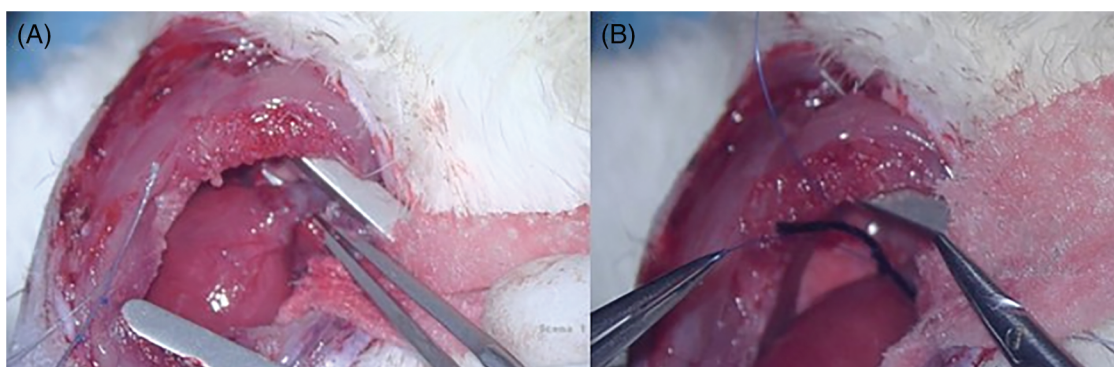

Figure 1: **A:** intraoperative picture showing the isolation of main pulmonary artery, as described in the main text. **B:** intraoperative picture showing the procedure of banding the main pulmonary artery, as described in the main text

2.3.3 Sham

SHAM operation consisted of a procedure that included anaesthesia, intubation, opening and closing of the chest, without performing the band placement. The rats of this group only experienced surgical stress.

2.3.4 Post-Operative Course

Animals were housed in cages, in a controlled air-conditioned space, in accordance with law. Tramadol 5 mg/kg was administered subcutaneously twice a day for the first 72 h post-surgery, then if needed. Animals were checked daily by animal care personnel and researchers, during the post-operative course. An evaluation system called "score pain system" (Table 2) was used for the identification of clinical signs of possible animals' suffering.

Table 2: Pain scoring system: all conditions need to be fulfilled

Clinical manifestation	Scoring
None	0
Ruffled fur	1
Ruffled fur, reduced physical activity	2
Ruffled fur, reduced physical activity and loss of weight between 10% and 15%	3
Ruffled fur, reduced physical activity, respiratory distress, and loss of weight between 15% and 20%	4
Ruffled fur, reduced physical activity, respiratory distress, loss of weight >20%, kyphosis	5

2.3.5 Sacrifice

Endpoints of the study were set at 5, 15, and whenever possible, 30 days. However, in case of evident illness, toxicity, physical deterioration, weight loss (>20% loss, compared to the weight measured the day of the surgery), the animals were immediately euthanized through their exposure to CO_2 for few minutes. Simultaneously, the abdomen and chest of these animals were opened to take samples of blood (from the abdominal aorta) and organs including spleen, liver and heart, which underwent further molecular and histopathological studies. Considering the fast growth of such animals, 30 days was estimated as an optimal time of follow up, corresponding to more or less 8–10 human months [12]. However, given the high mortality of this model, 15 days follow-up was considered as an acceptable endpoint.

2.4 Evaluation and Measures

2.4.1 Echocardiography

Echocardiography was performed using a Vevo 2100 system (Fujifilm Visual Sonics, Toronto, ON, Canada), equipped with a 30-MHz transducer. Anaesthesia was induced with 3% isoflurane and maintained with 1.5% isoflurane during constant monitoring of temperature, respiration rate, and ECG. Two-dimensional cine loops with frame rates of 200 frames per second of a long-axis view and a short-axis view at proximal, mid, and apical level of the LV were recorded. IVS and LV posterior wall thicknesses, LV internal diameter, and maximal LV length were measured in systole and in diastole from the long-axis B-mode image, according to standard procedures. EF was determined with the Simple method (Simpson monoplane): %EF = 100 × LV stroke volume/diastolic LV volume. Fractional shortening (FS) was calculated by measuring the percentage change in left ventricular diameter during systole. Gradient across the PAB was measured as previously reported [11]. Echocardiogram was performed at baseline, then 5 days, 15 days and 30 days, after each procedure, if the animal survived.

2.4.2 Morphological Analysis

The study protocol consisted of gross examination of cardiac specimens with images acquisition at the Olympus SZX12 stereoscope (Olympus, Tokyo, Japan). The method of investigation of excised hearts consisted of gross examination (heart weight), histology (presence of cardiomyopathic changes, necrosis, inflammation, replacement type fibrosis), and ultrastructure (basal membrane integrity, evaluation of mitochondria and loss of sarcomeric proteins).

2.4.3 Histology

Pathological studies were performed at the Anatomic pathology and Histology Unit of Padua. Hearts isolated after excision were weighed, and small fragments were sampled from both ventricles and the IVS for ultrastructural and molecular analysis. The samples were then fixed in 10% formalin buffered solution

for light microscopy (Olympus BX51 optical microscope), in 2% phosphate-buffered glutaraldehyde for transmission electron microscopy (TEM), and snap-frozen for molecular analysis. For histological analysis, 3–4 μm-thick paraffin-embedded sections were cut and routinely stained with haematoxylin and eosin (H&E) and Heidenhain's trichrome to examine the myocardium. To determine the presence of apoptosis, tissue sections were examined using the terminal deoxynucleotidyl transferase-mediated dUTP-biotin nick end-labelling method (TUNEL), as previously reported [13]. The apoptotic index was calculated as the percentage of positive nuclei in sections stained by TUNEL. Myocyte diameter in the short axis was measured on photomicrographs of haematoxylin and eosin-stained specimens at $40\times$ magnification, with the mean of multiple measurements calculated using Image Pro-Plus software. Measures were summarized using the mean $\pm$ standard deviation (SD) and compared between the case and control groups.

2.4.4 Transmission Electron Microscopy

Transmission electron microscopy (TEM) was used to characterize early lesions at cellular level. Small fragments of the hearts (2 mm × 2 mm) underwent to fixation in 2% phosphate-buffered glutaraldehyde. After glutaraldehyde fixation and osmium tetroxide post fixation, the samples were dehydrated in ascending ethanol series and embedded in epoxy resin. Semithin sections were stained with toluidine blue and observed at light microscopy. Ultrathin sections, after staining with uranyl acetate and lead citrate, were observed and photographed under Hitachi H7800 (Hitachi, Tokyo, Japan). Electron micrographs were taken by systematic random sampling and analysed in a blinded fashion.

2.4.5 Molecular Study

Blood samples underwent whole mRNA and microRNAs (miRNAs) isolation, quantification, and quality control. Whole miRNA sequencing by next generation sequencing (NGS) with Small-RNA Seq Library prep kit (Lexogen, Vienna, Austria) in a NextSeq platform (Illumina, San Diego, CA, USA). FASTQ files were processed by a bioinformatic pipeline with BaseSpace Labs (Illumina, San Diego). First, adapters were trimmed to obtain only miRNA reads. Subsequently, these reads were aligned to 4 reference databases: abundant, mature miRNA, other RNA and genomic. Finally, DESeq2 algorithm was used for differential expression analysis and over- and under-expressed miRNAs were identified in comparison with control group.

2.4.6 Sample Size

The primary objective of this pilot study was to inform the design and the feasibility of the main study, particularly in defining the prior distributions for a definitive experimental design defined in a Bayesian framework. Designing the trial using a Bayesian approach allows us to incorporate prior knowledge and continuously update our beliefs based on the previously data collected. This approach provides a more flexible and informative analysis, particularly beneficial in small sample studies, like this research context, by enabling direct probability statements about the hypotheses and accommodating uncertainty coherently [14]. We employed a Bayesian approach to determine the sample size for our main study. Assuming a medium effect size of 0.5 [15], a significance level of 0.05, and a desired power of 0.8, we used non-informative priors since this pilot study is intended to inform the Bayesian design of future trials. We performed iterative simulations in 1000 runs to calculate the proportion of experiments where the Bayes Factor exceeded 1 (absence of effect), adjusting the sample size until the desired power was achieved. This process resulted in a required sample size of 64 rats, distributed across four groups. This computation was performed using R 4.3.2. Designing the trial using a Bayesian framework allows us to incorporate prior knowledge and continuously update our beliefs based on the data collected. This approach provides a more flexible and informative analysis, particularly beneficial in small sample studies like ours, by enabling direct probability statements about the hypotheses and accommodating uncertainty

coherently. The pilot study is important for informing the sample size and design of future, more definitive experiments. However, pilot studies often require smaller sample sizes, typically around 10%–20% of the main study's sample size, or at least 12 rats per group, as provided by the literature, to deliver preliminary insights and test the feasibility of the research design [16]. Therefore, 49 rats were chosen to balance statistical power and practical constraints, ensuring sufficient data to refine the methodology and validate measurement tools.

2.4.7 Statistical Analysis

The sample has been described by reporting the median and the interquartile range of the age of the different study arms. Concerning mortality outcomes, the absolute number of deaths and mortality rates have been descriptively reported. Echocardiographic data were visually described by reporting the mean and SD per group and study time point for each functional parameter. The mean and SD have been calculated to define the prior parameters for a Normal-Normal model on the echocardiographic outcome, which will inform the experimental design of the main study. To compare the echo parameters across time in different groups, we estimated the Generalized Least Squares (GLS) model within a Bayesian framework. This serves as a preliminary proof of concept for establishing the prior distributions for the main study design. An illustrative example of this process is provided in the appendix. The GLS model accounts for potential heteroscedasticity by incorporating the inverse of the variances as fixed weights. Given the pilot and explorative nature of the study, and subsequently the limited sample size across experimental conditions, in the pilot phase, the interaction effects across the factorial design consisting of the time and treatment groups were not considered, and the effects were not adjusted for multiplicity issues or *post hoc* analyses performed. However, the overall intervention effect and time (5, 15, and 30 days) of GLS model effects have been estimated as preliminary proof of a possible PAB effect to be further explored in another research. Analyses were performed using R 4.3.2 [17] and brms package [18].

3 Results

3.1 Experimental Mortality

All rats treated with DOX exhibited decreased spontaneous motor activity, loss of body weight, ruffled dur, and decreased survival. As indicated in Table 3, similar to that described in the literature [9,10]:
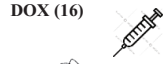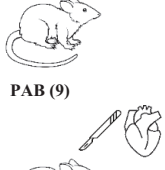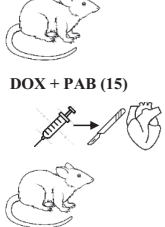
- for the DOX group, 4 rats reached the 5 days-endpoint, 3 rats reached the 15 days-endpoint and were sacrificed, and 2 rats reached 30 days and were sacrificed. 9 rats out of 16 died in the follow-up (mortality = 43.7%).
- for the DOX + PAB group (n = 15), eight rats reached the 5 days-endpoint and were sacrificed, five rats reached the 15 days-endpoint and were sacrificed and no rats reached the 30 days endpoint. Two rats died before the 30-days endpoint (mortality 13.3%)
- No deaths occurred in the PAB and SHAM groups.

Table 3: Protocol figure with methods and animals alive at each follow-up

GROUP (n)	5-DAYS ENDPOINT (n)	15-DAYS ENDPOINT (n)	30-DAYS ENDPOINT (n)
SHAM (9)	3	3	3

(Continued)

Table 3 (continued)

GROUP (n)	5-DAYS ENDPOINT (n)	15-DAYS ENDPOINT (n)	30-DAYS ENDPOINT (n)
DOX (16)	4	3	2
PAB (9)	3	3	3
DOX + PAB (15)	8	5	0

3.2 Echocardiographic Findings

As described before [11], the gradient across the band was measured in most of the animals, but it was not possible in all, due to technical reasons. Similarly to what measured at that time, the median PAB gradient in all animals was estimated to be 40 mmHg (range 35–50). Echocardiographic assessment confirmed that the DOX-induced DCM model involved functional derangement. On the other hand, among the eight DOX-treated rats undergoing PAB and surviving the procedure, 2D echocardiographic evaluation was performed in five rats a few days after the procedure, and in three rats at almost 15 days after surgery. When compared to post-DOX administration cardiac status, 2D echocardiography revealed an improved heart function after PAB that was statistically significant only for EF ($p = 0.01$) and FS ($p = 0.03$): EF and FS approached baseline conditions (Figs. 2 and 3), while we observed a trend towards a reduction in LV internal diameter and increased posterior wall and IVS thickness after PAB (Fig. 2). This effect was not statistically significant according to the GLS model estimation.

3.3 Histopathology Results

3.3.1 Gross Examination

The examination involved 4 hearts from rats treated with DOX undergoing PAB, 4 controls treated with DOX, and 4 treated with PAB without DOX. On gross examination hearts at all groups, cases and controls appeared normal, with a mean weight in controls after DOX treatment of 1.0 ± 0.3 g, in PAB post-DOX of 1.2 ± 0.1, in PAB without DOX of 1.5 ± 0.2 and in SHAM 1.1 ± 0.1. At transverse cut, no fibrosis was evident.
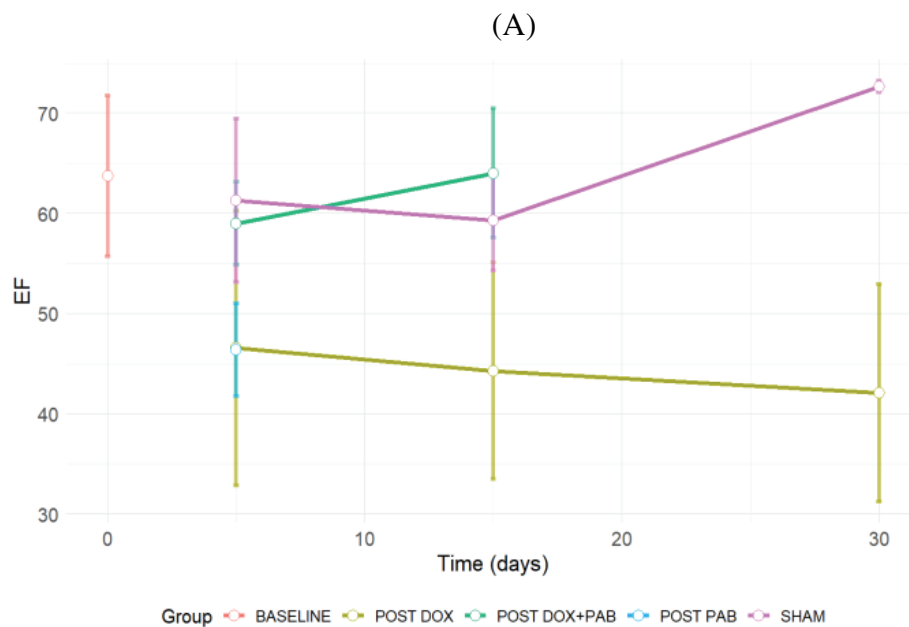
3.3.2 Histology

Both on routine histology and on semithin sections under the light microscope, no cardiomyopathic changes, inflammation, necrosis/apoptosis or replacement-type fibrosis in cases *vs.* controls were found. Only in PAB post-DOX and PAB without DOX treatment, we found diffuse pericarditis due to the surgical intervention (Fig. 4). TUNEL was completely negative in all the cardiac samples, cases and controls. The myocyte diameter in LV was 12.0 ± 0.98 μ in PAB after DOX, 11.75 ± 11.39 μ in PAB without DOX and 12.36 ± 3.97 μ in controls treated only with DOX.

3.3.3 Transmission Electron Microscopy

At ultrastructure, apoptotic myocytes were not seen in both cases and controls (no evidence of nuclear chromatin condensation and cytoplasmic shrinkage in the setting of an intact cytoplasmic membrane). Instead, characteristic structural alterations developed in cardiomyocytes treated with DOX (controls treated with DOX and PAB after DOX, but not in PAB controls without DOX) in terms of diffuse cytoplasmic vacuolization and loss of myofilaments with disorganization of the remaining bundles (Fig. 4). Interestingly, most mitochondria appeared normal with no evidence of swelling or lysis and normal morphology of the cristae, despite damage to the cytoplasm.

3.4 Molecular Results and Limitations

miRNA expression analysis was carried out in blood samples of DOX-treated rats and after PAB (DOX +PAB). Comparison analyses between either DOX-treated and sham or DOX-treated and DOX+PAB, did not highlight significant differences of miRNAs expression, which may reflect the small size effect of animals tested in each group (n = 3–5). Gene expression analysis was not warranted due to the absence of major structural evidences in the heart of DOX-treated and DOX+PAB treated rats.

(A)

	BASELINE	POST DOX	POST DOX	POST DOX	POST DOX+PAB	POST DOX+PAB	POST PAB	SHAM	SHAM	SHAM
DAYS	0	5	15	30	5	15	5	5	15	30
MEAN± SD, N	63.75 ± 8.01; n = 20	46.58 ± 13.72; n = 16	44.29 ± 10.81; n = 7	42.1 ± 10.86; n = 2	59 ± 4.14; n = 5	64 ± 6.46; n = 3	46.4 ± 4.64; n = 5	61.3 ± 8.14; n = 5	59.33 ± 5.03; n = 5	72.67 ± 0.58; n = 3

Figure 2: (Continued)

(B)

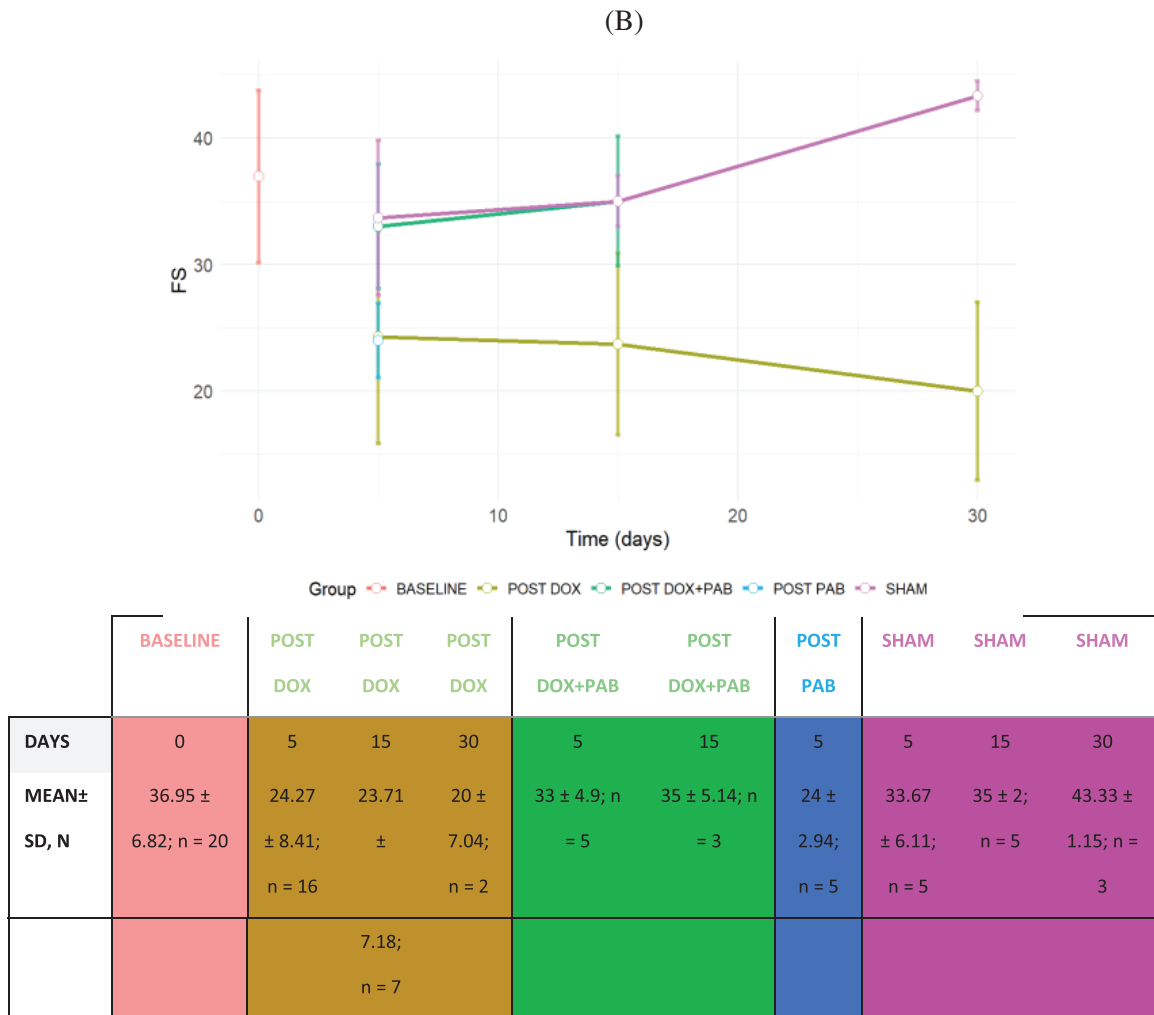|	BASELINE	POST DOX	POST DOX	POST DOX	POST DOX+PAB	POST DOX+PAB	POST PAB	SHAM	SHAM	SHAM
DAYS	0	5	15	30	5	15	5	5	15	30
MEAN± SD, N	36.95 ± 6.82; n = 20	24.27 ± 8.41; n = 16	23.71 ± 7.18; n = 7	20 ± 7.04; n = 2	33 ± 4.9; n = 5	35 ± 5.14; n = 3	24 ± 2.94; n = 5	33.67 ± 6.11; n = 5	35 ± 2; n = 5	43.33 ± 1.15; n = 3

Figure 2: Line Plot of LV Echo parameters of rats undergoing DOX-injection, DOX-injection + PAB, and SHAM at 5, 15, or 30 days. **A:** variations in EF; **B:** variations in FS. Data are expressed as mean ± SD. Legend: EF: Ejection Fraction; FS: fractional shortening. The sample size of groups (n) according to the follow-up time has also been reported
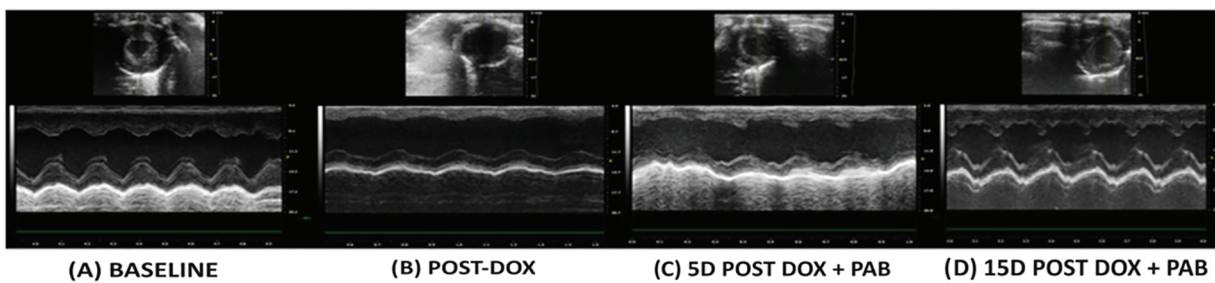

Figure 3: **A:** basal echo (short-axis) of one rat before DOX-injection and PAB, showing normal function; **B:** echo after DOX-injection, showing systolic dysfunction, with the flattening of the posterior wall and septum, as well as the increase of the RV and LV cavities; **C:** echo 5 days after PAB; **D:** 15 days after PAB, showing improved systolic function
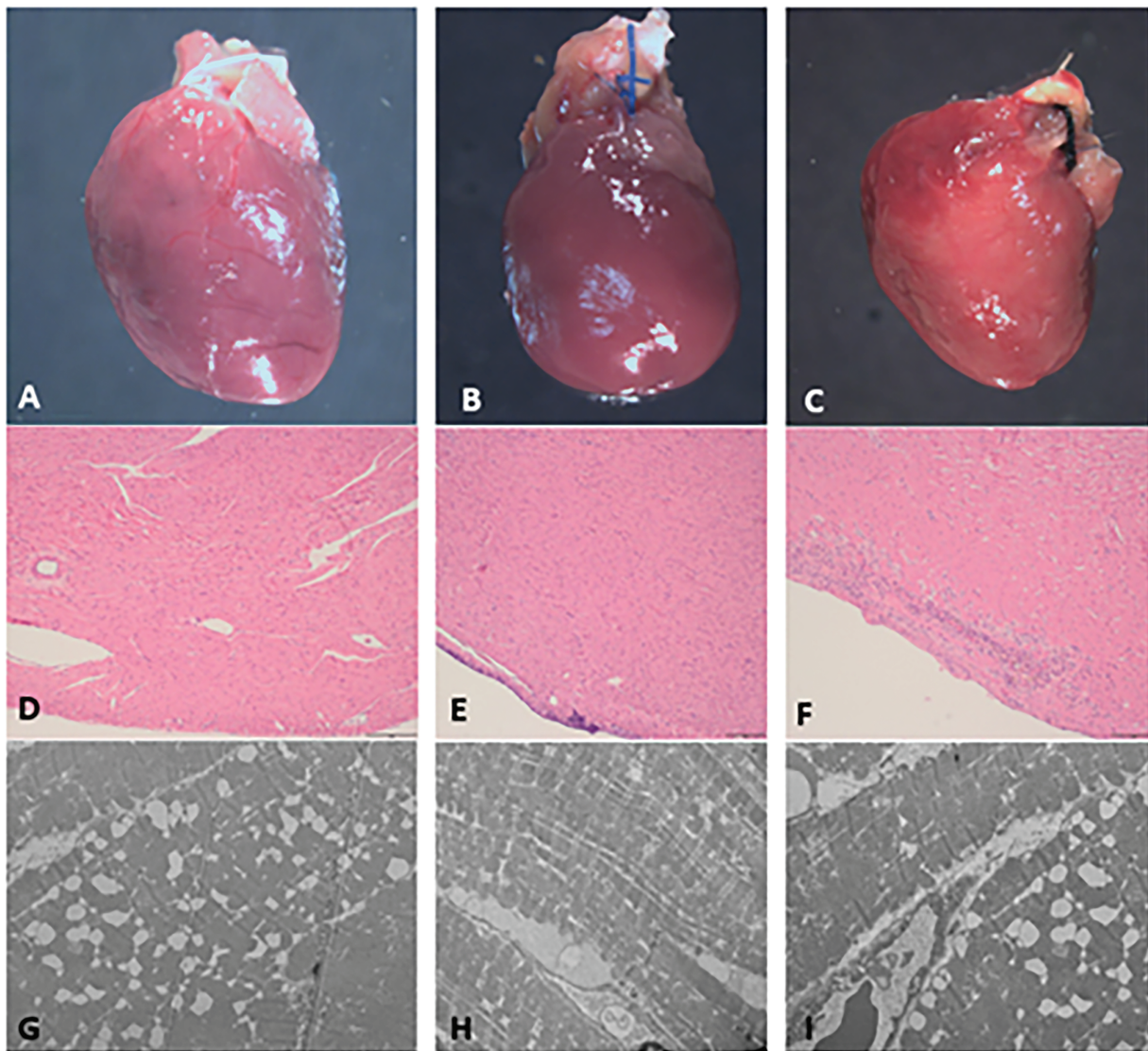
Figure 4: A, D, and G: rats treated with DOX. **A:** gross view of cardiac specimen without alteration; **D:** at histology (40× magnification, scale bar 100 μ), normal diameter and morphology of cardiomyocytes, in absence of inflammation, necrosis/apoptosis or replacement type fibrosis; **G:** at electron microscopy (2000× magnification, scale bar 5–10 μ), note cytoplasmic vacuolization of the cardiomyocytes with loss of sarcomeric proteins. **B, E, H:** healthy rat underwent PAB without previous DOX tratment. **B:** gross view of cardiac specimen without alteration, note PAB; **E:** at histology, only epicardial inflammation following surgical operation; **H:** ultrastructurally, no alteration of the cardiomycetes **C, F, I:** rat submitted to PAB after DOX treatment. **C:** gross view of cardiac specimen without alteration, note PAB; **F:** at histology, note epicardial inflammation following surgical operation; **I:** at electron microscopy, cytoplasmic vacuolization of the cardiomyocytes with loss of sarcomeric proteins following DOX treatment

4 Discussion

To the best of our knowledge, this is the first pilot experiment in the literature of a surgical experiment conducted on a rodent model with induced DCM undergoing a PAB to investigate ventricular rehabilitation.

The purpose of this model was to elucidate whether PAB is a feasible and reproducible procedure in a rodent model of pharmacologically induced DCM and to evaluate PAB-induced ventricular rehabilitation, underlying the observed effectiveness reported in clinical settings for infants and children with HF [4,5,19–21]. Despite its inherent advantages of simplicity and reduced cost, this experimental pilot study on rodent models revealed practical limitations.

As outlined in the literature [9], we encountered two major limitations associated with the DOX-induced DCM rat model: high mortality (approximately 50%) and significant individual variability in the extent of left ventricular remodeling and systolic dysfunction.

On the other hand, in our study no deaths occurred in the group of healthy rats undergoing only pulmonary artery banding. These results are consistent with those reported in the literature [11].

When PAB is performed on healthy rats, the procedure's mortality burden is null; however, when the rats have previously experienced the toxic systemic effects of DOX, the mortality after PAB is increased (13.3%), as an effect of synergistic stress. Overbanding or underbanding could also have an impact on mortality, even with the best efforts to measure the gradient. PAB turned out to be a reproducible procedure from a surgical point of view, but it was burdened by the morbidity caused by DOX on rats.

Nonetheless, we preliminary demonstrated an improvement in cardiac function five to fifteen days post PAB using 2D echocardiography.

In this study, SD rats were selected as the experimental model for DCM based on previous experiences with this model [22]. Despite their small size, the dimensions of their hearts and main vessels were adequate for the PAB procedure. The SD strain was chosen for its excellent reproductive performance, calm demeanor, and ease of handling.

Among the various experimental models of DCM, we opted for pharmacological induction through DOX injection due to its practicality and feasibility in our setting. Other models described in the literature include autoimmune myocarditis (EAM)-induced DCM [23], surgical induction through temporary left anterior descending artery (LAD) ligation [24], or pressure overload through ascending aorta constriction [25]. The latter two surgical models were not feasible in our laboratory due to current Italian experimental surgery legislation, which prohibits reoperations on experimental animals. Indeed, these models would have required two separate surgeries: one to induce left ventricular (LV) damage, which gradually progresses to decompensated heart failure (HF), and another to perform PAB.

No alterations were detected through standard histopathological and molecular tests. However, signs of cell damage were observed through transmission electron microscopy, indicating diffuse cytoplasmic vacuolization and loss of myofilaments with disorganization of the remaining bundles following DOX administration.

The short-term DOX protocol used to induce DCM in rats, though sufficient for detecting cardiac function alterations through 2D echocardiography and transmission electron microscopy, did not cause significant histopathological damage or variation in miRNA expression. This finding is consistent with Yerebakan's experience [6], who reported that echocardiography performed three months after PAB in sheep with HF induced by DOX revealed a better LV EF and FS than controls, as well as smaller LV dimensions. However, they also failed to demonstrate any difference in fibrosis or inflammatory infiltrate at terminal histopathology.

Several factors may contribute to this occurrence. Firstly, it could be attributed to the injection protocol, which reduces duration and associated costs but may not be adequate for establishing a robust DCM model. Furthermore, DOX-based HF does not replicate the exact pathological bases of DCM since it causes swelling and vacuolization of cardiomyocytes, disorganization of myofibrils, and diffuse fibrosis [8,9]. Moreover, experimental studies mainly focus on DOX's effects on the LV, while clinical experience in cancer

survivors indicates that anthracycline toxicity may also affect the RV [26]. Recent findings also suggest an increased production of free radicals in the RV myocardium of DOX-treated rats, revealing its possible biventricular toxicity [27]. Since preserved RV function is crucial for successful PAB application in DCM, the beneficial effects of PAB might be compromised in a DOX-based model of HF. Schranz speculated in clinical studies that ventricular hypertrophy induced by PAB could stimulate cardiac improvement through potential myocardial regeneration, particularly in younger patients [5]. Initially, our study aimed to establish a young and adult model of DOX-induced DCM, expecting better outcomes in the younger model with PAB treatment, hypothesizing myocardial regeneration. However, limitations emerged as young rats inevitably aged during the DOX administration period and displayed lower susceptibility to DOX's cardiotoxic effect. This observation aligns with the age-related difference in DOX pharmacokinetics described in the literature. In fact, DOX and its metabolites are increased in old rats due to reduced systemic clearance, which leads to a higher risk of anthracycline toxicity [28]. Additionally, sex differences were observed, with females being better protected from DOX-induced HF due to less mitochondrial damage associated with lower cardiotoxicity [29].

5 Conclusions

Creating a rodent model for DCM posed notable challenges, notably due to limited sample size stemming from high mortality post-DOX administration and pulmonary artery banding performed on rats which already suffered the toxic effects of the drug. Despite these hurdles, we managed to offer initial evidence of cardiac function decline via 2D echocardiography and transmission electron microscopy post-DOX injection. Additionally, echocardiographic assessment showcased cardiac function enhancement post-pulmonary artery banding, albeit without consistent support from histopathological and molecular analyses. These preliminary yet encouraging findings emphasize the necessity for another model which could be possibly associated to a lower mortality, for further exploration into the molecular signaling pathways involved and the potential for pulmonary artery banding to induce cardiac proliferation.

Author Contributions: Conceptualization, Massimo A. Padalino, Domenico Crea, Matteo Ponzoni, Arben Dedja; methodology, Arben Dedja, Domenico Crea, Matteo Ponzoni, Massimo A. Padalino; software, Domenico Crea, Danila Azzolina; validation, Alberto Cipriani, Riccardo Bariani, Kalliopi Pilichou, Maria Bueno Marinas, Stefania Rizzo, Danila Azzolina; formal analysis, Arben Dedja, Domenico Crea, Massimo A. Padalino; investigation, Massimo A. Padalino, Domenico Crea, Arben Dedja.; resources, Massimo A. Padalino.; data curation, Massimo A. Padalino, Domenico Crea, Danila Azzolina; writing—original draft preparation, Domenico Crea, Massimo A. Padalino; writing—review and editing, Massimo A. Padalino, Arben Dedja, Matteo Ponzoni, Alberto Cipriani, Stefania Rizzo, Kalliopi Pilichou, Maria Bueno Marinas, Danila Azzolina; visualization Domenico Crea, Massimo A. Padalino, Kalliopi Pilichou, Stefania Rizzo, Danila Azzolina; supervision, Massimo A. Padalino; project administration, Massimo A. Padalino; funding acquisition, Massimo A. Padalino. All authors reviewed the results and approved the final version of the manuscript.

Availability of Data and Materials: The datasets generated and/or analyzed during the current study are available from the corresponding author on reasonable request.

Ethics Approval: The study included animal subjects. It was approved by the Local Ethical (Body for Animal Welfare of the University of Padua) and received Ministerial Authorization (no. 24/2021-PR, released on 14 January 2021).

Conflicts of Interest: The authors declare no conflicts of interest to report regarding the present study.

References

1. Das BB. Current state of pediatric heart failure. Children. 2018 Jun 28;5(7):88. doi:10.3390/children5070088.

2. Towbin JA, Lowe AM, Colan SD, Sleeper LA, Orav EJ, Clunie S, et al. Incidence, causes, and outcomes of dilated cardiomyopathy in children. JAMA. 2006 Oct 18;296(15):1867–76. doi:10.1001/jama.296.15.1867.

3. Sinagra G, Merlo M, Pinamonti B, curatori. Dilated cardiomyopathy: from genetics to clinical management. Cham: Springer; 2019. Available from: http://www.ncbi.nlm.nih.gov/books/NBK553850/. [Accessed 2024].

4. Schranz D, Veldman A, Bartram U, Michel-Behnke I, Bauer J, Akintürk H. Pulmonary artery banding for idiopathic dilative cardiomyopathy: a novel therapeutic strategy using an old surgical procedure. J Thorac Cardiovasc Surg. 2007 Sep;134(3):796–7. doi:10.1016/j.jtcvs.2007.04.044.

5. Schranz D, Akintuerk H, Bailey L, Miera O, Danne F, Kavarana MN, et al. Pulmonary artery banding for functional regeneration of end-stage dilated cardiomyopathy in young children: world network report. Circulation. 2018 Mar 27;137(13):1410–2. doi:10.1161/CIRCULATIONAHA.117.029360.

6. Yerebakan C, Boltze J, Elmontaser H, Yoruker U, Latus H, Khalil M, et al. Effects of pulmonary artery banding in doxorubicin-induced left ventricular cardiomyopathy. J Thorac Cardiovasc Surg. 2019 Jun;157(6):2416–2428.e4. doi:10.1016/j.jtcvs.2019.01.138.

7. National Research Council (US) Committee for the update of the guide for the care and use of laboratory animals. In: Guide for the care and use of laboratory animals. 8th ed. Washington, DC, USA: National Academies Press (US); 2011. Available from: http://www.ncbi.nlm.nih.gov/books/NBK54050/. [Accessed 2024].

8. Cattapan C, Barbera MD, Dedja A, Pavan P, Salvo GD, Sabatino J, et al. Mechanical and structural adaptation of the pulmonary root after ross operation in a murine model. J Clin Med. 2022 Jun 28;11(13):3742. doi:10.3390/jcm11133742.

9. O'Connell JL, Romano MMD, Campos Pulici EC, Carvalho EEV, de Souza FR, Tanaka DM, et al. Short-term and long-term models of doxorubicin-induced cardiomyopathy in rats: a comparison of functional and histopathological changes. Exp Toxicol Pathol Off J Ges Toxikol Pathol. 2017 Apr 4;69(4):213–9.

10. Vasić M, Lončar-Turukalo T, Tasić T, Matić M, Glumac S, Bajić D, et al. Cardiovascular variability and β-ARs gene expression at two stages of doxorubicin—induced cardiomyopathy. Toxicol Appl Pharmacol. 2019 Jan 1; 362:43–51. doi:10.1016/j.taap.2018.10.015.

11. Vida VL, Dedja A, Faggin E, Speggiorin S, Padalino MA, Boccuzzo G, et al. The effects of basic fibroblast growth factor in an animal model of acute mechanically induced right ventricular hypertrophy. Cardiol Young. 2012 Aug;22(4):436–42. doi:10.1017/S1047951111002034.

12. Sengupta P. The laboratory rat: relating its age with human's. Int J Prev Med. 2013 Jun;4(6):624–30.

13. Gavrieli Y, Sherman Y, Ben-Sasson SA. Identification of programmed cell death *in situ* via specific labeling of nuclear DNA fragmentation. J Cell Biol. 1992 Nov;119(3):493–501. doi:10.1083/jcb.119.3.493.

14. Chow SC, Chang M. Adaptive design methods in clinical trials—a review. Orphanet J Rare Dis. 2008 May 2;3:11. doi:10.1186/1750-1172-3-11.

15. Cohen J, Statistical power analysis for the behavioral sciences. Hillsdale, NJ, USA: Lawrence Erlbaum Associates, Inc.; 1977.

16. Julious SA. Sample size of 12 per group rule of thumb for a pilot study. Pharm Stat. 2005;4(4):287–91. doi:10.1002/pst.v4:4.

17. R Core Team. R: a language and environment for statistical computing. Vienna, Austria: R Foundation for Statistical Computing; 2015.

18. Bürkner PC. Advanced bayesian multilevel modeling with the R package brms. R J. 2018;10(1):395–411. doi:10.32614/RJ-2018-017.

19. Ponzoni M, Frigo AC, Castaldi B, Cerutti A, Salvo GD, Vida VL, et al. Surgical strategies for the management of end-stage heart failure in infants and children: a 15-year experience with a patient-tailored approach. Artif Organs. 2021 Sep 12;45(12):1543. doi:10.1111/aor.v45.12.

20. Ponzoni M, Zanella L, Reffo E, Cavaliere A, Pozza A, Castaldi B, et al. Late left ventricular myocardial remodeling after pulmonary artery banding for end-stage dilated cardiomyopathy in infants: an imaging study. Int J Cardiol. 2023 Sep 1;386:160–6. doi:10.1016/j.ijcard.2023.05.040.

21. Di Candia A, Castaldi B, Bordin G, Cerutti A, Reffo E, Biffanti R, et al. Pulmonary artery banding for ventricular rehabilitation in infants with dilated cardiomyopathy: early results in a single-center experience. Front Pediatr. 2020;8:347. doi:10.3389/fped.2020.00347.

22. Vida VL, Angelini A, Ausoni S, Bilardi A, Ori C, Vlassich F, et al. Age is a risk factor for maladaptive changes in rats exposed to increased pressure loading of the right ventricular myocardium. Cardiol Young. 2007 Apr 1;17(2):202–11. doi:10.1017/S1047951107000376.

23. Schmerler P, Jeuthe S, h-Ici DO, Wassilew K, Lauer D, Kaschina E, et al. Mortality and morbidity in different immunization protocols for experimental autoimmune myocarditis in rats. Acta Physiol Oxf Engl. 2014 Apr;210(4):889–98. doi:10.1111/apha.2014.210.issue-4.

24. Chen J, Chemaly ER, Liang LF, LaRocca TJ, Yaniz-Galende E, Hajjar RJ. A new model of congestive heart failure in rats. Am J Physiol-Heart Circ Physiol. 2011;301(3):H994. doi:10.1152/ajpheart.00245.2011.

25. Weinberg EO, Schoen FJ, George D, Kagaya Y, Douglas PS, Litwin SE, et al. Angiotensin-converting enzyme inhibition prolongs survival and modifies the transition to heart failure in rats with pressure overload hypertrophy due to ascending aortic stenosis. Circulation. 1994 Sep;90(3):1410–22. doi:10.1161/01.CIR.90.3.1410.

26. Boczar KE, Aseyev O, Sulpher J, Johnson C, Burwash IG, Turek M, et al. Right heart function deteriorates in breast cancer patients undergoing anthracycline-based chemotherapy. Echo Res Pract. 2016 Sep;3(3):79. doi:10.1530/ERP-16-0020.

27. Rahmanifard M, Vessal M, Noorafshan A, Karbalay-Doust S, Naseh M. The protective effects of coenzyme Q10 and lisinopril against doxorubicin-induced cardiotoxicity in rats: a stereological and electrocardiogram study. Cardiovasc Toxicol. 2021 Nov;21(11):936–46. doi:10.1007/s12012-021-09685-8.

28. Teraoka K, Hirano M, Yamaguchi K, Yamashina A. Progressive cardiac dysfunction in adriamycin-induced cardiomyopathy rats. Eur J Heart Fail. 2000;2(4):373–8. doi:10.1016/S1388-9842(00)00111-2.

29. Sexual Dimorphism of Doxorubicin-Mediated Cardiotoxicity | Circulation: Heart Failure. Available from: https://www.ahajournals.org/doi/10.1161/CIRCHEARTFAILURE.114.001180?url_ver=Z39.88-2003&rfr_id=ori:. [Accessed 2024].